Correlation effects in quasi-one-dimensional quantum wires

Luke Shulenburger,[1] Michele Casula,[1] Gaetano Senatore,[2,3] and Richard M. Martin[1]
[1]*Department of Physics, University of Illinois at Urbana-Champaign, 1110 W. Green Street, Urbana, Illinois 61801, USA*
[2]*INFM-CNR DEMOCRITOS National Simulation Center, Trieste, Italy*
[3]*Dipartimento di Fisica, Teorica dell' Università di Trieste, Strada Costiera 11, 34014 Trieste, Italy*
(Received 19 May 2008; published 6 October 2008)

We explore the role of electron correlation in quasi-one-dimensional quantum wires as the range of the interaction potential is changed and their thickness is varied by performing exact quantum Monte Carlo simulations at various electronic densities. In the case of unscreened interactions with a long-range $1/x$ tail there is a crossover from a liquid to a quasi-Wigner crystal state as the density decreases. When this interaction is screened, quasi-long-range order is prevented from forming, although a significant correlation with $4k_F$ periodicity is still present at low densities. At even lower electron concentration, exchange is suppressed and the electrons behave like spinless fermions. Finally, we study the effect of electron correlations in the double quantum wire experiment [Steinberg *et al.*, Phys. Rev. B **73**, 113307 (2006)] by introducing an accurate model for the screening in the experiment and explicitly including the finite length of the system in our simulations. We find that decreasing the electron density continuously drives the system from a liquid to a state with quite strong $4k_F$ correlations. This crossover takes place around 22 μm^{-1}, near the density where the electron localization occurs in the experiment. The charge and spin velocities are also in good agreement with the experimental findings in the proximity of the crossover. We argue that correlation effects play an important role at the onset of the localization transition.

DOI: 10.1103/PhysRevB.78.165303 PACS number(s): 73.21.Hb, 71.45.Gm, 71.10.Pm

I. INTRODUCTION

It is well known that the effect of interactions in quasi-one-dimensional (Q1D) systems of electrons, usually called "quantum wires," is enhanced compared to higher dimensional systems. There are universal properties described by the Luttinger liquid paradigm, the *effective* low energy theory which applies for strictly one-dimensional (1D) models,[1–5] such as spin-charge separation, charge localization, and conductance quantization. However, the microscopic details, such as the width and type of the transverse confinement or the distance and shape of neighboring screening media, can have a large impact on the properties of the Q1D systems as they are very sensitive to the effective interaction. These systems can be realized in semiconductor structures, where there are elegant experimental studies,[6–12] and it is essential to describe the system accurately for a realistic comparison of theory and experiment.

In this paper we study how the thickness, finite size, and screening affect the phase boundaries of some universal features with a particular emphasis on the charge localization and spin properties. We address the issue of how the electron correlation depends upon the microscopic details parametrized in the interaction using ground-state quantum Monte Carlo (QMC) methods[13] such as diffusion Monte Carlo,[14,15] and its lattice regularized version[16] which are ideal numerical tools to study Q1D systems, since they provide exact results in one dimension. Previous QMC studies regarded the determination of the Luttinger liquid (LL) parameters for a Q1D system with screened interactions[17] and the ground-state properties of a model with a long-range Coulomb potential.[18] Here we compare various model interactions in a unified picture, with the final goal of quantifying the role of correlation in the localization transition found by Steinberg *et al.*[12]

With this aim it is particularly important to include both the effects of the long-range Coulomb potential and the consequences of its screening in the interactions. In dimensions larger than 1, the $1/x$ tail of the Coulomb pairwise potential leads to a Wigner crystal phase of the homogeneous gas at low densities when the potential energy dominates over the kinetic contribution.[19–21] In this regime the spin exchange drops to an exponentially small value[22] as the overlap between unlike spin particles is exponentially suppressed by the localization of the electrons. Therefore, one of the signatures of the liquid-to-crystal transition is a decrease in the spin stiffness. However, it is possible that other spin and charge phases could exist in between.

In 1D the situation is radically different. It is well known that a Luttinger liquid with $1/x$ interactions exhibits slowly decaying charge-charge correlations, but no true long-range order, as the quantum fluctuations are stronger in lower dimensions.[5] Nonetheless there should be a crossover from a high-density liquid to a low-density regime with quasi-long-range charge order also called a "fluctuating Wigner crystal" (Ref. 23). However the LL theory does not predict where the crossover happens, as the correlation function parameters are not universal but depend on the details of the interaction. Also the interplay between charge and spin is quite unclear. Indeed the LL parameters depend on the effective one-dimensional potential in a nontrivial way. For instance, the spin properties are strongly affected by its short-range behavior which includes the effect of the thickness, as the transverse dimension can effectively tune the spin exchange. On the other hand, the quasiorder of the charge degrees of freedom is stabilized by the long-range tail. The relative importance of the short versus long-range correlations is set by the microscopic model of the system. Recently Fogler[24,25] proposed that a correlated state with very small spin exchange exists for ultrathin wires at densities *between* the liquid and

the quasi-Wigner crystal phase. In the limit where the short-range part can be effectively described by an infinite repulsive contact interaction, this state can be related to a *noninteracting* spinless Fermi system as in the Tonks-Girardeau gas.[26] In a one-dimensional system of fermions, the coexistence of strong short-range repulsions and very long-range interactions leads to a peculiar state, which Fogler termed a Coulomb-Tonks gas.

In previous theoretical work, quantitatively accurate studies of the liquid-to-crystal one-dimensional crossover have been carried out only for inhomogeneous systems, with longitudinal extension controlled by an external confinement, and where the finite (and very small) size allows one to solve the problem by means of exact diagonalization.[27–29] However, the broken translational symmetry leads to quite different properties, particularly in the charge and spin-density profiles.

From the experimental side, technological advances in the preparation of cleaved edge overgrowth samples have enabled tunneling measurements between two high mobility parallel wires, which probe striking features such as the spin-charge separations in the excitation spectra.[10] In a recent extension of the tunneling experiments, Steinberg *et al.*[12] applied a gate to the upper wire in order to tune its electron density by charge depletion. Below a critical threshold, measurements revealed a dramatic transition which can be interpreted as the onset of localization in the wire. Although it is believed that the transition is mainly driven by electron-electron interaction effects as the liquid phase is in a ballistic regime, so far there is no agreement between the critical density predicted by theory and the actual experimental value. Some features of the experiment, such as the fringes of the differential conductance in the liquid phase and the first two peaks of the tunneling current in the localized phase, have been explained in an independent-particle picture[7,8] and at the mean-field level.[30] The LL theory has been applied to describe the general features of the tunneling current in the Wigner state by assuming a spin incoherent regime.[31] However it is unclear at which density the spin degrees of freedom become incoherent, as the spin velocity measured in the experiment is in disagreement with previous numerical estimates. Another open issue is related to the fact that only a small fraction of electrons take part in the localized state. It is clear that an accurate microscopic description of the experimental situation is necessary to account for all these features. In our study we include the most important details such as an accurate screening and the effect of the finite size of the wire to correctly describe and understand the physics underlying the experiment.

Throughout the paper we use units of the effective Bohr radius $a_0^\star = \frac{\hbar^2 \epsilon}{m^\star e^2}$ for length and the effective Rydberg $\mathrm{Ryd}^\star = \frac{e^2}{2\epsilon a_0^\star}$ for energy, where ϵ is the dielectric constant of the embedding medium and $m^\star$ is the effective electron mass.

The paper is organized as follows: In Sec. II we present results for a quasi-one-dimensional electron gas (1DEG) with long-range $(1/x)$ interactions for different densities $\rho = \frac{1}{2r_s}$ and thicknesses. We carefully study the liquid-to-quasicrystal crossover by varying the Wigner-Seitz radius r_s which sets the relative importance of the kinetic energy and the interaction. By means of QMC techniques, we also study the charge compressibility and the spin susceptibility in order to analyze the interplay between the charge and spin properties of the wire. The effect of the wire's thickness on the crossover and the spin properties is taken into account by performing simulations with three different wire widths. In Sec. III we compare the unscreened $1/x$ potential with an interaction screened by a metallic plane. In Sec. IV we interpret the localization transition found in the series of two wire tunneling experiments[6–12] by studying the evolution of liquid-to-crystal correlations in a finite wire with interactions effectively screened by another parallel wire. We make a comparison between the finite system and the corresponding homogeneous infinite system interacting with the same potential. We also show the agreement between our model and the experiment. Finally in Sec. V we summarize our results and comment on possible refinements to our calculations.

II. UNSCREENED COULOMB INTERACTIONS

We study a system of electrons interacting via the Coulomb $(1/x)$ potential which are confined to one dimension by a harmonic potential in the transverse direction $V(r_\perp) = \frac{r_\perp^2}{4b^4}$, where b tunes the thickness of the wire. This system was previously studied using QMC by Casula *et al.*[18] and here we follow the conventions used in that work. We integrate over the transverse degrees of freedom, which is a good approximation when the density of electrons in the wire is low ($r_s \gg \pi b/4$), and hence the longitudinal energy scale is small compared to the excitation energies related to the perpendicular motion. This integration yields an effective one-dimensional interaction $V_b(x) = \frac{\sqrt{\pi}}{b}\exp(\frac{x^2}{4b^2})\mathrm{erfc}(\frac{|x|}{2b})$, which has a long-range $1/x$ tail. The thickness b of the wire controls the short-range behavior of the potential, which is finite at the origin $[V(0) = \sqrt{\pi}/b]$. Since the crossover between the short and long-range behaviors is at $x \approx b$, for smaller b the repulsion is stronger as the particles approach each other.

In this work we have chosen to study three different thicknesses: $b = 1$, 0.1, and 0.0001. The first two values correspond to typical experimental thicknesses for semiconductor quantum wires, whereas the last one is chosen to explore the ultrathin limit as studied analytically by Fogler[24,25] and experimentally realized in carbon nanotubes placed on $SrTiO_3$ substrates.[32,33] For each value of b, the density in the wire $(\frac{1}{2r_s})$ is varied, allowing for the interaction strength to change and the corresponding ground-state properties are computed.

We use diffusion Monte Carlo (DMC) and lattice regularized diffusion Monte Carlo[16] (LRDMC) methods to project the initial variational ansatz to the ground state $|\Psi_0\rangle$. These methods are particularly suited to the simulation of one-dimensional fermions. Indeed, the well-known "sign problem" does not affect these calculations as the nodes are fully determined by the points of coincidence between the electrons and therefore are exactly included in the trial wave function $|\Psi_T\rangle$. Since the final DMC or LRDMC distribution is the product of the true ground state and the trial wave function, some observables such as the density and the structure factor are determined using the forward walking

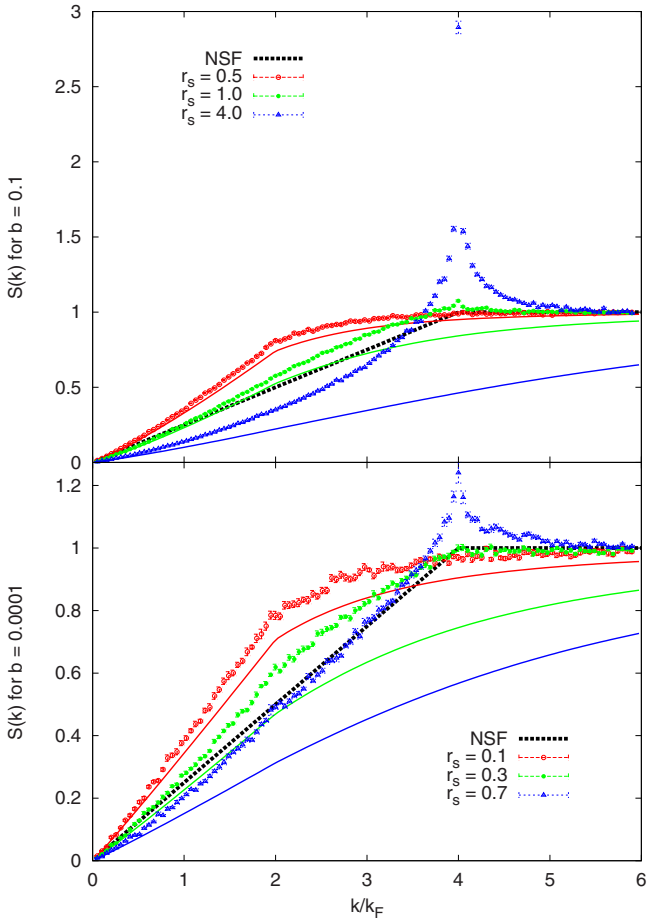

FIG. 1. (Color online) Structure factor for $b=0.1$ (upper panel) and $b=0.0001$ (lower panel), computed for a system with 78 electrons. The QMC (dotted) and MSA (solid lines) structure factors are reported for different densities (r_s). Also the noninteracting spinless fermion (NSF) structure factor is drawn (solid black line) for comparison.

technique[34,35] in order to generate unbiased expectation values. The errors reported in our results are only due to statistical fluctuations inherent in the Monte Carlo sampling of the wave function, and they can be made arbitrarily small by increasing the simulation length.

We simulate an unpolarized wire with N electrons subject to periodic boundary conditions. The trial wave function is written in the Slater-Jastrow form

$$\Psi_T = D^{\uparrow}D^{\downarrow}\exp\left[-\sum_{i<j}u(x_{ij})\right], \tag{1}$$

where the Slater determinants for up and down spin electrons read

$$D^{\sigma}(x_1^{\sigma},\ldots,x_{N^{\sigma}}^{\sigma}) = \prod_{1\le i<j\le N^{\sigma}}\sin\left[\frac{G}{2}(x_i^{\sigma}-x_j^{\sigma})\right], \tag{2}$$

with $G=2\pi/L$ and $L=2r_sN$ the length of the simulation cell. We follow Ref. 36 to determine the Jastrow function $u(x)$. Its Fourier components are

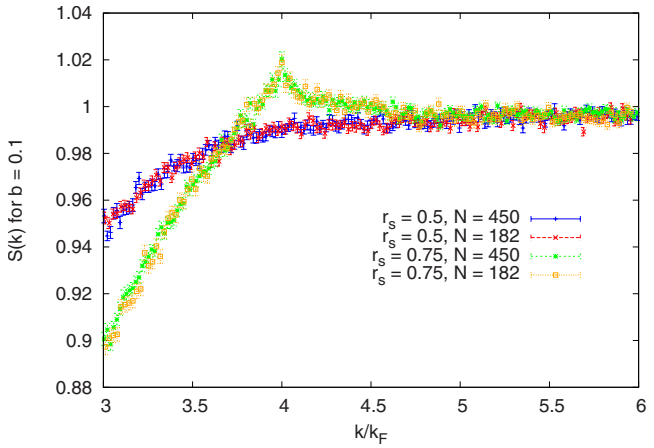

FIG. 2. (Color online) Detail for the structure factor near $4k_F$ for $b=0.1$, computed for $N=182$ and $N=450$ at two densities ($r_s=0.5$ and $r_s=0.75$) in the proximity of the crossover from a liquid to a quasicrystal.

$$2\rho\tilde{u}(k) = -S_0(k)^{-1} + \sqrt{S_0(k)^{-2} + 2\rho\tilde{V}_b(k)/k^2}, \tag{3}$$

with $S_0(k)=(k/2k_F)\theta(2k_F-k)+\theta(k-2k_F)$ the structure factor of a noninteracting 1DEG, $\rho=\frac{1}{2r_s}$ the density, and $\tilde{V}_b(k)$ the Fourier transform of $V_b(x)$. To reduce the finite-size effects in our simulation we use the Ewald technique to sum our potential as discussed in detail in Ref. 18. This approach has been used to study the infinite wire with the long-range potential $V_b(x)$ and also the screened potentials described in Secs. III and IV. In the latter case, the sum over the images has been done numerically in the real space as the potentials have a shorter range.

To reveal the presence of charge ordering in the system, we first analyze the static structure factor $S(k)=\frac{1}{N}\langle\rho(-k)\rho(k)\rangle$, where $\rho(k)=\Sigma_j e^{ikr_j}$ are the Fourier components of the electron density. At high density the structure factor is very similar to the mean spherical approximation[37] (MSA) prediction $S_{\mathrm{MSA}}(k)=S_0(k)/[1+2\rho\tilde{u}(k)S_0(k)]$ as expected (see Fig. 1), since in the limit $r_s\to 0$ the MSA becomes exact.[18] Specifically, there is no peak at $4k_F$ up to $r_s=0.5$ ($r_s=0.2$) for $b=0.1$ ($b=0.0001$), namely, there are no correlations with the mean interparticle spacing (Fig. 2). As the density decreases, a peak develops at $4k_F$. This peak is a necessary feature for a one-dimensional quasi-Wigner crystal and it is absent in the MSA prediction which has no structure at $4k_F$. For $b=0.1$ we carried out simulations with up to 450 particles for $r_s=0.5$ and $r_s=0.75$ to check the convergence of the $S(k)$ in the liquid regime close to the onset of the $4k_F$ charge correlations (Fig. 2).

The scaling of the height of the $4k_F$ peak of $S(k)$ with the number of particles (reported in Fig. 3 for $b=0.1$) highlights the features of a liquid-to-quasicrystal crossover. When the peak is absent there is no significant dependence of the $S(4k_F)$ value as a function of system size, however when there is a peak in the structure factor at $4k_F$, its scaling is sublinear, signaling a quasi-long-range order (linear scaling would indicate a true Wigner crystal). The points in Fig. 3 are fit very well by a functional form obtained from the

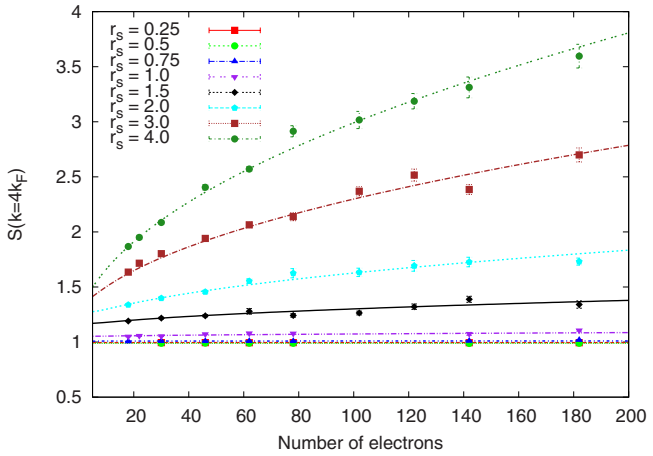

FIG. 3. (Color online) Scaling of the $4k_F$ component of the structure factor with respect to the number of particles. The scaling is reported for various densities with $b=0.1$. The lines are the best fit of the function in Eq. (4) given by the LL theory.

charge-charge correlation function[38] derived by Schulz[23] in the LL framework with long-range interactions

$$\int_{c_0}^{L} dx\, \exp(-i4k_F x)\langle\rho(0)\rho(x)\rangle = aL\, \exp(-4c\sqrt{\log L}) + b, \tag{4}$$

where we explicitly include the dependence on the system size L by taking the Fourier transform over the simulation cell. The short-distance cutoff c_0 is introduced because the LL theory provides only the asymptotic behavior for $\langle\rho(0)\rho(x)\rangle$. Further logarithmic corrections could be included[39] in Eq. (4), but we take just the leading-order expansion, which should be the most relevant for the system sizes computed here. One would need much larger systems which are beyond our current numerical capabilities to resolve further corrections. The bosonization formalism gives a parameter dependent scaling for the $4k_F$ component of $\langle\rho(0)\rho(x)\rangle$ which is left undetermined in the LL theory and depends on the details of the interaction. At high densities there is no peak in the structure factor and the electron gas is liquid (Fig. 2). Consequently, there is no finite-size dependence at $4k_F$ and the parameter a undetermined in the LL theory is zero.

We also determine the charge compressibility κ and the spin susceptibility χ of the electron gas. To compute κ we used two techniques. The first is to apply the definition of that quantity as the reciprocal of the second derivative of the total energy with respect to the density r_s. Our QMC calculations provide measurements of the total energy, so these derivatives can be taken by fitting our data with a suitable functional form. The error in such a determination comes from both the statistical uncertainty in the calculations and the constraint represented by the choice of the fitting function. As a technical detail, it is also necessary to extrapolate the energy to the thermodynamic limit which can be a costly proposition. Nevertheless, we can compute the charge compressibility, and validate the second method to evaluate κ, using the parametrization in Ref. 18, which holds for a system with fixed polarization $\zeta=(N^{\uparrow}-N^{\downarrow})/N$ and depends only on r_s. The spin susceptibility χ will be considered in a separate publication where the energy as a function of polarization ζ will be presented.[40] The other method we use to compute both κ and χ is to calculate the momentum resolved excitation energies of the system and exploit the sum rules which *exactly* relate the collective modes of the long-wavelength spectrum with κ and χ. It is possible to derive the following relations:[41]

$$\omega_\rho(k\to 0) = v_F|k|\sqrt{\rho_F V(k\to 0) + \frac{\kappa_0}{\kappa}}, \tag{5}$$

$$\omega_\sigma(k\to 0) = v_F|k|\sqrt{\frac{\chi_0}{\chi}}, \tag{6}$$

where $\omega_\rho(k)$ $[\omega_\sigma(k)]$ is the energy of the lowest charge (spin) excitation with momentum k, ρ_F is the density of states of the free-electron gas at the Fermi energy, and κ_0 and χ_0 are its charge compressibility and spin susceptibility, respectively.

In order to find out the lowest energy states of a given momentum k we employ a method proposed by Ceperley and Bernu,[42] which is a generalization of the transient estimate used in the projection Monte Carlo (DMC or LRDMC) framework. This method is based on the idea that it is possible to compute the excitation spectrum of a system in a direct and variational way by projecting the initial basis functions to their lowest energy state with the given symmetry. In our case the basis set is the Feynman ansatz,[43] i.e., $\rho(k)|\Psi_0\rangle\,\forall\,k$ for the charge excitations and $\sigma(k)|\Psi_0\rangle\,\forall\,k$ for the spin excitations, where $\sigma(k)=\Sigma_j\Sigma_\sigma\sigma e^{ikr_j^\sigma}$ is the Fourier transform of the spin density. In the following we assume to work with the charge excitations, but the same applies for $\sigma(k)$. Since the basis set is orthogonal, the method in Ref. 42 is greatly simplified, as every k component is decoupled. For each k, we have to calculate

$$\frac{\langle\Psi_0|\hat{\rho}(k,\tau)\hat{H}\hat{\rho}(-k,0)|\Psi_0\rangle}{\langle\Psi_0|\hat{\rho}(k,\tau)\hat{\rho}(-k,0)|\Psi_0\rangle} = \frac{\sum_i \epsilon_k^i A_k^i e^{-\tau(\epsilon_k^i - E_0)}}{\sum_i A_k^i e^{-\tau(\epsilon_k^i - E_0)}}, \tag{7}$$

where $\hat{\rho}(k,\tau)$ is written in the Heisenberg representation with imaginary time evolution, $|\Psi_k^i\rangle$ is the ith excited state with momentum k, ϵ_k^i is its energy, $A_k^i=|\langle\Psi_k^i|\rho(-k)|\Psi_0\rangle|^2$ is the spectral weight of the eigenvalue expansion, and E_0 is the ground-state energy. For large τ the ratio in the above equation will converge to the lowest energy ϵ_k^0 of a given k, provided A_k^0 is nonzero. Another limitation is given by the exponentially small denominator, which will exponentially increase the statistical noise of the estimate as the projection time increases. Both the numerator and denominator in Eq. (7) are evaluated by means of the forward walking[34,35] procedure based on the DMC or LRDMC sampling. Indeed, for large enough τ the left—hand side of Eq. (7) can be rewritten as

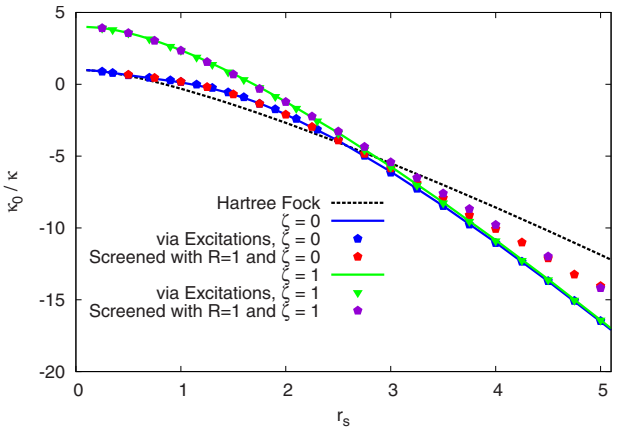

FIG. 4. (Color online) Inverse charge compressibility κ_0/κ of the unpolarized and fully polarized wire for $b=0.1$, with both screened ($R=1$) and unscreened interactions. Also the HF (dashed black line) charge compressibility is reported for the unpolarized wire. The solid lines are obtained from the second derivative of the energy parametrization, while the points are evaluated through the charge excitations as explained in Sec. II. The statistical error in the determination of the charge compressibility is approximately 0.02 in these units and is comparable with the point size.

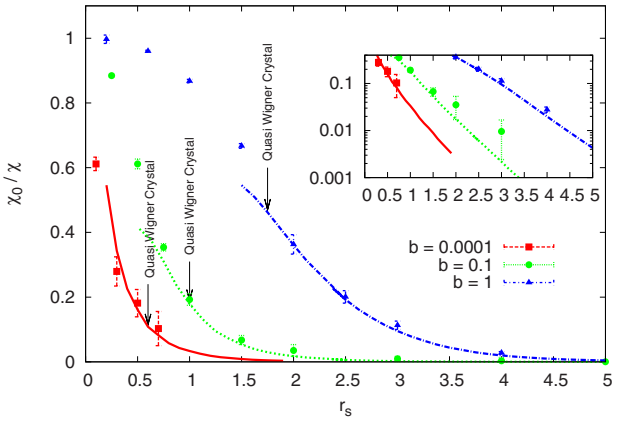

FIG. 5. (Color online) Inverse spin susceptibility χ_0/χ for different thicknesses. The dependence on r_s is shown. The points are the QMC calculations, while the lines are the WKB estimates. The arrows indicate the liquid-to-quasi-Wigner crystal crossover which is determined by the onset of the $4k_F$ peak in the static structure factor. Our estimate of the crossover density (r_s^*) has an uncertainty due to the statistical fluctuations in the calculation of the static structure factor and the actual r_s values we have studied.

$$\frac{\int dr_1 dr_2 \rho(-k) G(r_1, r_2, \tau) E_L(k, r_2) \rho(k) P(r_2)}{\int dr_1 dr_2 \rho(-k) G(r_1, r_2, \tau) \rho(k) P(r_2)}, \tag{8}$$

where $E_L(k,r)=\frac{H\rho(k)\Psi_T(r)}{\rho(k)\Psi_T(r)}$ is the local energy of $\rho(k)|\Psi_T\rangle$, $P(r)=\Psi_T(r)\Psi_0(r)$ is the QMC mixed distribution, and $G(r_1,r_2,\tau)=\Psi_T(r_1)\langle r_1|e^{-\tau H}|r_2\rangle/\Psi_T(r_2)$ is the importance sampled Green's function.

Because the excitation energies $\omega(k)=\epsilon_k^0-E_0$ are computed relative to the ground-state energy E_0, there is a cancellation of errors since the sample generated to compute E_0 and ϵ_k^0 is the same. Therefore a modest size calculation is enough to get converged energies. The convergence with the propagation time can be more difficult to obtain. However, for the long wavelengths $\rho(k)|\Psi_0\rangle$ is a good approximation to the lowest excited state with momentum k and the energies can be determined easily with a short projection time τ. When the small k range of energies is fit to the form in Eqs. (5) and (6), κ and χ are determined. The results for the charge compressibility obtained with this method agree with the second derivatives of the total energy in all cases we have made the comparison, as is shown in Fig. 4.

The knowledge of κ and χ can shed more light on the properties of the liquid-to-quasicrystal crossover. By looking at the charge compressibility (Fig. 4), it is apparent that the role of the electron correlation is becoming increasingly important in the proximity of the crossover, where there is significant discrepancy between the Hartree-Fock (HF) and QMC values of κ. In particular, the correlation makes the system *softer* than the HF, which is consistent with a more pronounced localization of the electrons. At even lower densities the charge compressibility of the unpolarized system is approaching that of a fully polarized (or spinless fermion) gas. The difference between the two is going exponentially to zero and they almost overlap for $r_s>4$ (with $b=0.1$). This means that the energy of the spin excitations is getting smaller and smaller as the density decreases. This feature is revealed by the inverse spin susceptibility χ. The χ_0/χ ratio is plotted in Fig. 5. This value becomes exponentially small at low densities, where it is difficult to get a statistically accurate QMC estimate, since the sampling of the spin is "frozen" by the presence of quasinodes (pseudonodes) between unlike spin electrons.[18] The strong interaction causes the electrons to repel each other at short range, and the corresponding wave function is very small at the coalescence points of electrons with opposite spin. Consequently the spin-flip rate in the QMC sampling becomes small and the efficiency decreases. However the charge properties do not seem to be affected by this slowing down. The physical reason for the quasinodes will become even more apparent in Sec. III, when we will discuss the Tonks-Girardeau physics of the screened wire.

In the low-density regime where exact Monte Carlo sampling becomes difficult the WKB approximation is useful for determining the dynamical properties of the electron gas. Following the example of Matveev[44] we use the WKB approximation to determine the rate at which two electrons exchange by calculating the energy barrier that they must overcome. Although fluctuations prevent the formation of a Wigner crystal, the equilibrium positions of the electrons are assumed to be equally spaced with periodicity $2r_s$. Central to the accuracy of this approximation is the fact that at low densities the tunneling is dominated by the effect of the potential, and the statistics can be ignored. Furthermore, all electrons are treated as uncorrelated except for a single pair which is allowed to exchange. In contrast to Matveev's approach we assume that the other electrons are distributed about their equilibrium positions according to the harmonic

approximation with a Gaussian spread instead of being fixed delta function point particles. Taking the initial positions of the two exchanging electrons to be at $x=0$ and $x=2r_s$, they feel a static potential given by

$$V_{\mathrm{WKB}}(x) = \sum_{n\neq 0,1} \int_{-\infty}^{\infty} \rho(y) V(x - 2nr_s + y) dy, \tag{9}$$

where $\rho(y)=\sqrt{\alpha/\pi}\exp(-\alpha y^2)$ is the equilibrium charge density of the nonexchanging electrons and $V(x)$ is the interparticle potential. The harmonic approximation gives $\alpha = \sqrt{m\frac{\partial^2 W(x)}{\partial x^2}}$, where $W(x)$ is the potential at a given lattice site due to an infinite array of electrons spaced as $2r_s$.

At low densities the electrons behave as a spin chain obeying the Heisenberg Hamiltonian were the spin flips are mediated by an exchange of nearest-neighbor electrons, so the spin susceptibility can be determined from the energy barrier computed within the WKB approximation by analogy with the Heisenberg Hamiltonian in 1D as shown by Matveev.[44] The spin velocity of the equivalent Heisenberg spin chain can be found from the Bethe ansatz solution,[45,46] yielding $v_\sigma = \pi J r_s$, where J is the size of the energy barrier in the WKB approximation. This gives the susceptibility through Eq. (6).

Where the density is large enough that QMC reliably samples the spin exchanges the spin susceptibility computed using the forward walking techniques agrees well with the WKB estimate only after the smearing of the electron sites given by the harmonic approximation. It is therefore important to use the potential in Eq. (9) to have an accurate estimate of the exchange at intermediate densities. This agreement and the fact that the dynamical many-body corrections to the WKB estimate are very small at low density[47] justify the use of WKB for dilute systems where it is difficult to extract information from the QMC calculations. In addition, the exponential decay of v_σ versus $\sqrt{r_s}$ obtained in this way is in agreement with previous results[44,48,49] for potentials where they can be compared.

Figure 5 summarizes our findings for the unscreened wire. The liquid-to-quasicrystal crossover is shifted to higher densities for thinner wires, while the spin susceptibility is always significantly different from zero in the crossover region for the values of the confinement taken into account. The smallest b we studied ($b=0.0001$) corresponds to one of the thinnest confinements realized experimentally.[32,33] The spin exchange is still sizable in the crossover region due to the not-so-long localization length of the electrons and not-so-thin width of the wire. Therefore, in our study we did not find any signature of the Coulomb-Tonks gas phase in between the liquid and quasi-Wigner crystal, which was claimed by Fogler for ultrathin wires.[25] However, the structure factor plotted in Fig. 1 reveals the tendency for electrons to approach the noninteracting spinless fermion behavior (the limit where the Coulomb-Tonks gas picture holds) as the wire width decreases. The fundamental difference with respect to the noninteracting spinless picture is the pronounced peak at $4k_F$, which characterizes the Coulomb long-range interactions at low density.

III. SCREENED INTERACTIONS IN GATED WIRES

The primary interest of this paper is to model a quantum wire formed in semiconducting nanodevices. In that case there is almost always a metallic gate that screens the long-range $(1/x)$ potential. To see the changes that such a gate would cause, we introduce a perfectly conducting metal plane parallel to the wire located a distance R away. Using the electrostatic method of images the potential is constructed by assuming that a wire is placed at a distance $2R$ from the original one with the same particle distribution but opposite sign. The equation for this potential is

$$V(x) = \int\int d\vec{r}d\vec{r}' \frac{\rho_b(\vec{r})\rho_b(\vec{r}')}{\sqrt{(\vec{r}-\vec{r}')^2 + x^2}} - \int\int d\vec{r}d\vec{r}' \frac{\rho_b(\vec{r})\rho_b(\vec{r}')}{\sqrt{(\vec{r}-\vec{r}'-2\vec{R})^2 + x^2}} = V_b(x) - V_{\mathrm{int}}(x,R), \tag{10}$$

where $\vec{r}$ and $\vec{r}'$ are transverse vectors and $\rho_b(\vec{r}) = \frac{1}{b\sqrt{2\pi}} \times \exp(-\frac{r^2}{2b^2})$ is the ground-state charge distribution of a two-dimensional harmonic oscillator with the wire's confining potential $V_{\mathrm{wire}}(r) = \frac{r^2}{4b^4}$. The first integral gives the effective unscreened interparticle potential $V_b(x)$ described in Sec. II and the second one is the potential due to the image charge on the screening wire $V_{\mathrm{int}}(x,R)$.

The quasi-Wigner crystal correlations derived by Schulz[23] apply only when the interaction is long range $(1/x)$. In the case of the screened interaction above the potential decays as $4R^2/x^3$ at large distances, so a simple scaling argument shows that the Wigner crystal correlations should be absent at very low densities. Indeed, if $r_s > 8R^2/\pi$ the typical kinetic energy of the electrons, the Fermi energy E_F, is larger than the potential energy computed at the mean interparticle distance $(2r_s)$. At these low densities Matveev[44] has pointed out that it is possible to map the screened short-range interaction into a repulsive contact potential

$$V(x) = U\delta(x), \tag{11}$$

where the constant U is chosen so the delta function potential and the screened one have equal transmission coefficients. On the other hand, in the density range $1 \ll r_s < 8R^2/\pi$ the $1/x$ shoulder of the potential can induce $4k_F$ correlations, which are strong but not strong enough to stabilize any sort of quasiorder. Calculations of the finite-size scaling of the $4k_F$ peak of the structure factor for $b=0.1$ and $R=200$ show the saturation of its height for $N \gtrsim 100$, and so demonstrate the absence of the quasi-Wigner crystal correlations when screening is introduced despite quite a large distance to the metallic gate (Fig. 6). Only in the limit of $R \to \infty$ does one recover the unscreened potential and the possibility for a quasi-long-range charge order.

The lack of the quasi-Wigner crystal state does not change the crossover to the spinless fermion physics present in the unscreened system. Even though the quasi-long-range charge order is absent at low densities, the charge compressibility still approaches that of a gas of spinless fermions as the density decreases. This approach can be seen in Fig. 4. It is

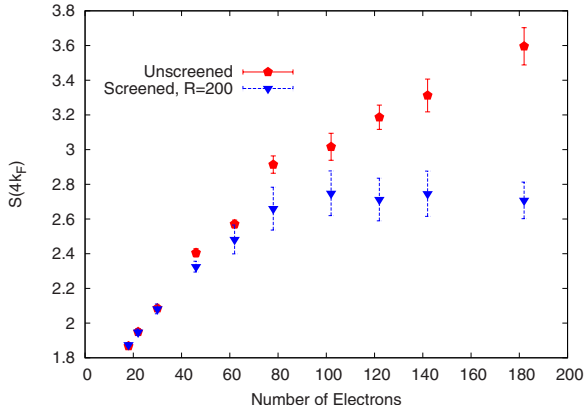

FIG. 6. (Color online) Scaling of the $4k_F$ component of the structure factor with respect to the number of particles for $b=0.1$ and $r_s=4$. For comparison, the scaling is reported for the unscreened V_b interaction and the screened potential in Eq. (10) with $R=200$.

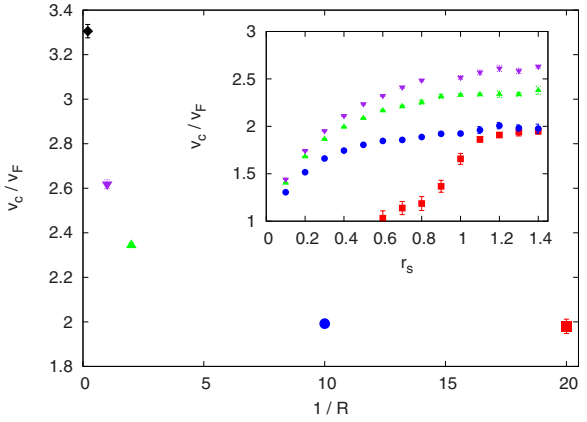

FIG. 7. (Color online) Asymptotic large r_s values of the charge velocity in units of v_F vs inverse screening length for ultrathin wire ($b=0.0001$) from $R=0.05$ to $R=5$. In the inset we report the full dependence of the charge velocities on r_s at different R.

therefore clear that the spin crossover does not depend on the long-range correlations. In fact, this crossover can be reproduced by a system of electrons interacting via the delta function interaction in Eq. (11) where the constant U is large, an interaction that has no long-range piece whatsoever.

The low-density limit with screened interactions is particularly interesting as the screening introduces a new feature. At low densities the electron-electron repulsion at short range makes exchanges between electrons virtually impossible, corresponding to the limit $U\to\infty$. As a result for the ultrathin wire with strong screening ($b\ll 1$ and $r_s\gg 8R^2/\pi$), the mapping of the interaction to the potential in Eq. (12) becomes *exact*. In this situation not only do the electrons behave as spinless fermions, but the charge velocity approaches that of *noninteracting* spinless fermions ($v_\rho=2v_F$). This is analogous to the case of bosons with infinite repulsive contact interactions, (or impenetrable particles) where the system can be mapped into a noninteracting Fermi gas.[26] The impenetrable Bose system is often called a Tonks-Girardeau gas. In our case the situation is analogous, namely, the fermions become impenetrable due to an effective infinite contact repulsion, and so they behave as they were noninteracting and spinless. We refer to this behavior as Tonks-Girardeau regime. One of its features is the presence of nodes in the wave function at the coalescence of unlike spin pairs. This is the extreme case when the pseudonodes that complicate the ergodicity of Monte Carlo calculations at low density as reported in Sec. II become actual nodes.

While this effect has been discussed in the literature,[24,25,44] our work provides quantitative predictions for the onset of the noninteracting spinless behavior. Figure 7 shows the charge velocity in the limit of low density for different values of the screening in the thinnest wire we studied ($b=0.0001$). We found that in order for the Tonks-Girardeau behavior to manifest itself, the distance to the gate R must be less than 0.1 and the density must be lower than $r_s=1$. For R larger than 0.1, at low density the charge velocity does not converge to the noninteracting spinless fermion limit ($2v_F$), but saturates at a larger value.

It is possible to see the transition of the screened electron gas to the noninteracting spinless fermion behavior more directly by analyzing the static structure factor, as was done in the unscreened case. In Fig. 8, the $S(k)$ is plotted at different densities for the ultrathin wire with $b=0.0001$ and gate located at $R=0.1$ from the wire. Contrary to the case of the unscreened wire (Fig. 1 lower panel), at low densities the peak at $4k_F$ is absent and the structure factor approaches that for noninteracting spinless fermions quite closely. Notice that at the same time the charge velocity approaches the value of $2v_F$ (see Fig. 7).

The same study was repeated for the wire with $b=0.1$. Here the short-range behavior of the potential is much less repulsive than in the $b=0.0001$ case and the same value R for the screening. The result of this is that the charge velocity does not converge to $2v_F$ even for a gate as close as $R=0.1$, which equals the width of the wire and thus represents the geometric limit of validity for the uncorrelated interwire interaction. Therefore for $b=0.1$ and thicker wires, whose widths are realizable in semiconducting nanostructures, we did not find the Tonks-Girardeau behavior in our calculations.

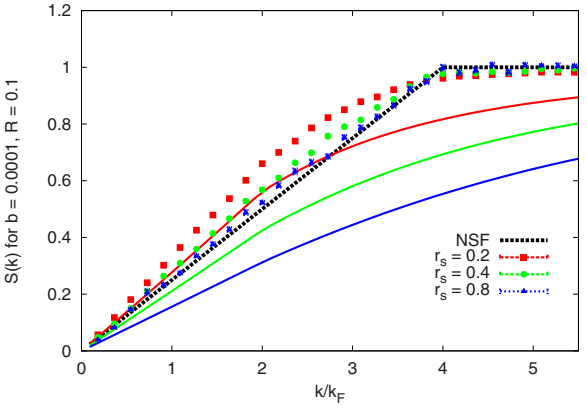

FIG. 8. (Color online) Static structure factor for the screened wire with $b=0.0001$ and $R=0.1$, plotted for three values of the density $r_s=0.2$, 0.4, and 0.8. The solid lines correspond to the MSA prediction for each density and the black line is the structure factor for noninteracting spinless fermions. The magnitude of the error bars is comparable with the point size.

IV. LOCALIZATION TRANSITION IN TWO PARALLEL GaAs WIRES

Quasi-one-dimensional systems can be realized in GaAs/AlGaAs heterostructures by means of various techniques. One such technique is cleaved edge overgrowth, which has been applied recently to build an experimental setup with two parallel wires so that it is possible to observe momentum resolved tunneling from one to the other.[6–12] In this series of experiments both the energy of the tunneling electrons and their momentum could be tuned by changing the relative chemical potential and the applied magnetic field. This setup allows the dispersion relations of each wire to be probed in a quite straightforward manner. Steinberg *et al.*[12] further explored how this tunneling is affected by a gate that depletes the density of the electrons in the upper wire. They found that as the density is decreased there is a marked transition in the tunneling interpreted as a transition from a liquid to a localized state.

In the experiment, the center to center distance between the two wires is $R=31$ nm. The upper wire is 2 μm long and 20 nm wide. It is the probe to study the electron localization. The electrons tunnel from the lower wire, which has a width of 30 nm and is taken to be infinitely long. This is also a screening medium for the upper wire. The system is fabricated out of GaAs for which $\epsilon=13.1$ and the effective electron mass is $m^\star=0.067m_e$. This gives an effective Bohr radius $a_0^\star=\frac{\epsilon\hbar^2}{m^\star e^2}\approx 10$ nm. For the experiment in question the electron density in the lower wire is around 60 $\mu\mathrm{m}^{-1}$, which corresponds to $r_s=0.83$ in $a_0^\star$ units, while in the upper wire the density is varied by tuning the gate voltage V_G. The effect of V_G on the lower wire is very small[12] and can be neglected.

The results presented in Sec. III offer an avenue to explore the role of the electron correlation in the transition observed in the experiment. As the density in the wire decreases the strength of the potential increases relative to the kinetic energy. One effect of this increased relative strength is that exchanges between the electrons are suppressed, causing the system to crystallize. To better quantify the importance of this effect in the experimental system, in this section we take into account a more realistic potential, assuming the electrons are screened by the lower wire instead of an infinite metallic gate. To construct this interaction we neglect the correlation between the wires and treat the screening effects coming from the electrons in the lower wire within the linear-response theory. We write the potential in Fourier space

$$V(k,R) = V_b(k) + V_{\mathrm{int}}(k,R)\chi(k)V_{\mathrm{int}}(k,R), \tag{12}$$

where $V_b(k)$ and $V_{\mathrm{int}}(k,R)$ defined in Eq. (10) are the intra- and interwire potentials, respectively. $V_{\mathrm{int}}(k,R)$ is evaluated by assuming that the thickness of the two wires is the same (and equal to the upper wire). This significantly simplifies the form and the calculation of the interwire interaction. $\chi(k)$ is the static density-density response function of the lower wire, taken in the random-phase approximation (RPA)

$$\chi_{\mathrm{RPA}}(k) = \frac{\chi_0(k)}{1 - V_{b'}(k)\chi_0(k)}, \tag{13}$$

where $\chi_0(k)=\frac{1}{\pi k}\ln\left|\frac{k-2k_F}{k+2k_F}\right|$ is the static response function for a one-dimensional noninteracting Fermi gas and b' is the width of the lower wire. The experimental geometry sets the parameters in our quasi-one-dimensional interaction $V(k,R)$. The confinement potential for the upper wire is chosen so that the electrons are constrained to be inside the 10 nm thick wire. Specifically, we require that the radial root mean squared displacement is equal to the lithographic thickness yielding $b=0.707(\approx 1/\sqrt{2})$ for the upper wire. The choice of confinement also agrees well with the experimental observation that a second mode becomes populated at $n=80$ $\mu\mathrm{m}^{-1}$.[6] Similarly, the lower wire's thickness is given by $b\prime=1.061$ $(\approx 1.5/2)$. The distance between the wires is $R=3.0$, while the Fermi momentum in the RPA response function for the lower wire is set by the density $r_s=0.83$.

Our screened potential in Eq. (12) is similar to that used by Fiete *et al.*,[31] who chose a perfect metal response function which is valid when the screening wire is at very high densities. Here we use the RPA which depends on the experimental density of the lower wire through the value of the Fermi momentum k_F. We notice that our screened potential equals that in Ref. 31 at $k=2k_F$ and in the limit of small k, namely, the long-range tail is the same, decaying approximately as $1/x^{5/4}$.

We first analyze the homogeneous system and then explicitly include a longitudinal confinement in our simulations to quantify the finite-length impact on the properties of the system and more closely reproduce the experimental situation. In the homogeneous system of electrons interacting via the potential in Eq. (12), we observe the appearance of a $4k_F$ peak in the $S(k)$ around $r_s=2.2$. As shown in Fig. 9, it is clearly visible for $r_s>2.6$, whereas no peak is discernable for $r_s\leq 1.9$. This crossover is similar to that found for long-range $1/x$ interactions. However, the important difference here is that the quasi-long-range order is not present in this case. Indeed, we have made a systematic study of the scaling with size, and the height of the peak converges to a finite value in the thermodynamic limit for all densities taken into account. This behavior is consistent with the decay of the screened interaction which is *faster* than $1/x$.[23] Therefore, the crossover is between a high-density liquid to one with strong $4k_F$ correlations, whose onset can be related to the transition occurring in the experimental system. We observe that the experiment is performed in a rather strong magnetic field, which is used to tune the momentum of the tunneling electron. Since the spin susceptibility is large in the proximity of the crossover, as we have seen previously for the unscreened wire, it is likely that the wire will be partially or fully polarized in the experimental setup. For a more quantitative argument, one should look at the energies of the polarized and unpolarized states, which are provided for the unscreened wire.[18] In any case, in order to have an idea of the effect of the spin polarization on the crossover density, we have also performed simulations at $\zeta=0.75$. A partial spin polarization is used to allow the physics due to the singulari-

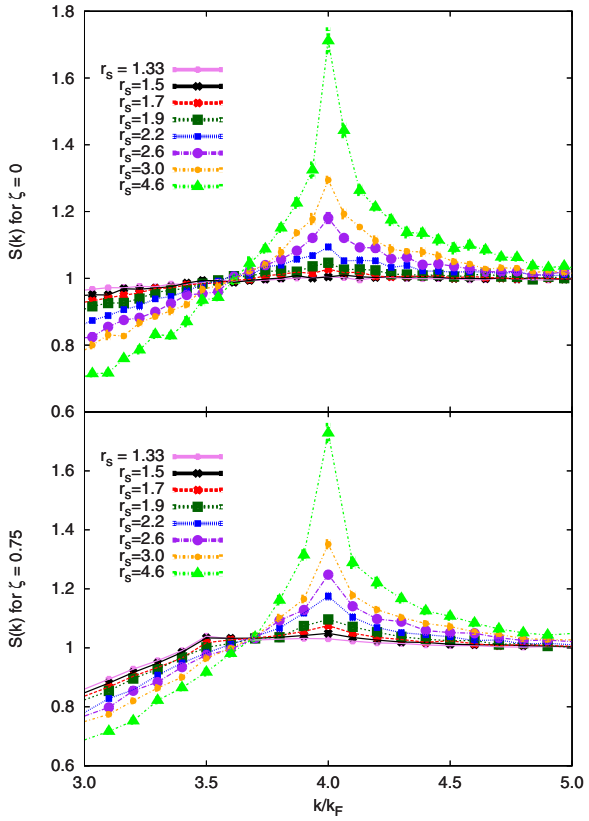

FIG. 9. (Color online) Static structure factor for a homogeneous wire with $b=0.707$ interacting with the effective potential in Eq. (12), which includes the screening by another homogeneous wire with $r_s=0.83$, $b=1.061$, and $R=3$. The structure factor is plotted for several values of the upper wire density, with r_s ranging from 1.7 to 4.6 and also for two values of the spin polarization with $\zeta=0$ and $\zeta=0.75$. The calculations have been converged to the thermodynamic limit, requiring $N=62$ for $r_s \leq 3.0$ and $N=78$ for $r_s=4.6$ subject to periodic boundary conditions. The structure factor has been plotted versus k/k_F, where k_F is the Fermi momentum in the unpolarized electron gas. The similarities of the peak heights at $4k_F$ for both values of ζ show the relative insensitivity of the crossover to spin polarization. The shoulder in $S(k)$ for the high-density curves with $\zeta=0.75$ is due to the Fermi surface of the majority species of electrons.

ties of the structure factor at the Fermi surface to be disentangled from the physics due to the mean interparticle spacing, which is directly related to the $4k_F$ correlations. As one can see in Fig. 9, the crossover density is insensitive to the spin polarization, at least in this strongly correlated regime.

The above treatment of the upper wire as infinite and homogeneous can be improved to resemble the experiments more closely. In the study of the 1DEG there are strong effects due to any perturbation that breaks the translational invariance of the system. For instance, Tserkovnyak *et al.*[7] showed that the asymmetry in the oscillations of the conductance as a function of the momentum transferred between the two wires can be explained at the WKB level by having a soft confinement potential for the upper wire. In a later paper they accurately determined the functional form of the longitudinal confinement by fitting its parameters to reproduce the period of those oscillations as a function of the magnetic field applied to the sample.[8] The potential that provided a good fit to their data reads

$$V(x) = E_F\left(\frac{2x}{L}\right)^8, \tag{14}$$

where E_F is the Fermi energy of the upper wire and L is approximately 1.5 times the lithographic length of the upper wire, namely, $L=300$ in $a_0^\star$ units.

We used the above potential together with the interparticle potential in Eq. (12) to study the effect of the confinement on the transition. Although in principle diffusion Monte Carlo yields an unbiased ground-state energy in one dimension even for a confined system (the nodes being exactly determined by the coalescence conditions just as in the infinite homogeneous wire), in practice it is necessary to improve the guidance wave function to reduce the variance of our estimates. The Jastrow factor used in the homogeneous system [Eq. (3)] is replaced by a more sophisticated factor including one-, two-, and three-body terms, fully optimized by means of the stochastic reconfiguration (SR) algorithm,[50,51] while the Slater part is kept the same as in Eq. (1). The one-body Jastrow $\exp(J_1)$ is needed to localize the electrons in the finite system. It reads

$$J_1 = \sum_{i=1}^{N} (-\alpha x_i^4 - \beta x_i^5), \tag{15}$$

where α is a free parameter and $\beta=\sqrt{E_u}(2/L)^4/5$ is fixed to cancel the contribution of the potential to the local energy at the leading order in the large distance expansion. The two-body $\exp(J_2)$ and three-body $\exp(J_3)$ Jastrow factors are given by

$$J_2 = \sum_{(i\sigma)<(j\sigma')} u_2^{\sigma\sigma'}(x_{ij}) \tag{16}$$

and

$$J_3 = \sum_{(i\sigma),(j\sigma'),(k\sigma'')} u_3^{\sigma\sigma'}(x_{ij}) u_3^{\sigma'\sigma''}(x_{jk}), \tag{17}$$

where x_{ij} is the interparticle distance. Since the finite system with screened interactions is dominated by short-range correlations, we chose $u_n(x)$ to have a simple Gaussian form

$$u_n^{\sigma\sigma'}(x) = \delta_n^{\sigma\sigma} \exp(-x^2/\gamma_n^{\sigma\sigma'}), \tag{18}$$

with $\delta_n^{\sigma\sigma'}$ and $\gamma_n^{\sigma\sigma'}$ variational parameters. Energy minimization improves the quality of the variational wave function and stabilizes the forward walking estimate[35] of the expectation values on the DMC projected state.

Again the static structure factor is determined for different densities of electrons in the upper wire. In contrast to the calculations for the homogeneous system, the density of the electrons is not a direct input to the calculation. Instead, we control the number of electrons in the wire which are then free to relax according to the external potential. An average density can be determined by considering the locations of the $2\tilde{k}_F$ and $4\tilde{k}_F$ peaks of the structure factor and comparing their value to those of an infinite array of electrons $2\tilde{k}_F=\frac{\pi}{2\tilde{r}_s}$ and

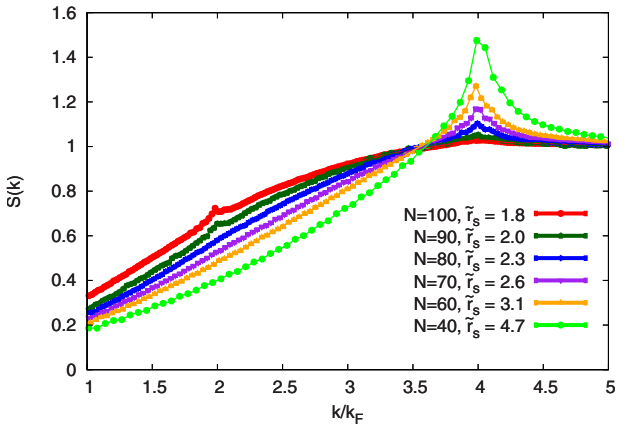

FIG. 10. (Color online) Static structure factor for a wire as in Fig. 9, but with finite length. $S(k)$ is plotted for 40, 60, 70, 80, 90, and 100 electrons. The corresponding effective densities $\tilde{r}_s$ are reported in the legend. The magnitude of the error bars is comparable with the point size.

$4\tilde{k}_F=\frac{\pi}{\tilde{r}_s}$, $\tilde{r}_s$ being the effective density in the system. Using these conventions, the structure factor for several different numbers of electrons is plotted in Fig. 10.

In addition to the formation of a broad peak in the $S(k)$ at $4k_F$ around $N=80$, which corresponds to $\tilde{r}_s=2.3$, the density profile $n(x)=\langle\Sigma_i\delta(x-x_i)\rangle$ of the electrons also shows a clear cut sign of the transition. At low densities, the electrons are distributed in order to minimize the interparticle repulsion. This leads to N oscillations in the density profile of the wire, a configuration also called "Wigner molecule," (Ref. 52) which corresponds to the $4k_F$ peak in the $S(k)$. When the density is increased, the number of peaks in the density profile is reduced by a factor of 2, the Pauli exclusion principle between like spin particles is the only factor that prevents the electrons form crossing each other. At the same time the $4k_F$ peak in the $S(k)$ disappears and only a $2k_F$ singularity is present. The density is plotted in Fig. 11 for half of the wire as the system is symmetric under inversion around its center. This plot also suggests a transition near $N=80$.

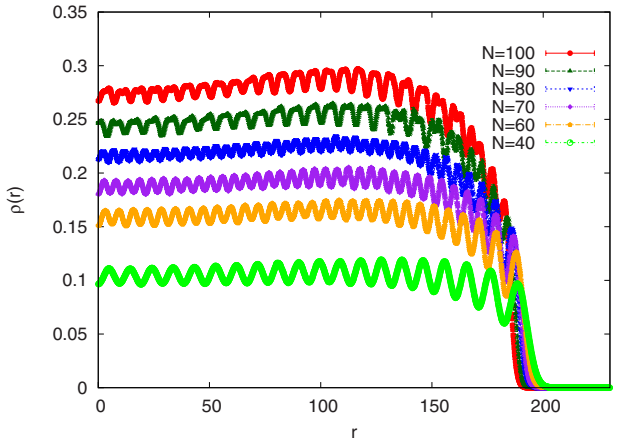

FIG. 11. (Color online) Density profile for electrons in the finite wire as in Fig. 10, plotted for half of the wire length. $N=40$, 60, 70, 80, 90, and 100 are considered.

Surprisingly, the calculations with the confinement potential and the infinite wire give very similar structure factors in the vicinity of the transition, suggesting that the interparticle correlations are not strongly affected by the external confinement at those densities. At lower densities the peak at $4k_F$ is much larger for the homogeneous system because of the limited number of particles in the finite wire. Both the infinite and finite wires show a transition from a system with $2k_F$ correlations to a state where correlations have a $2r_s$ periodicity. The crossover occurs around $r_s=2.3$, which corresponds to the density of 22 μm^{-1} in a GaAs heterostructure. This is very close to the density found by Steinberg *et al.* (20 μm^{-1}) for the localization transition in wires where one subband is occupied. However it seems that in the experiment the localization involves only few particles (up to 12 in the highest density localized state), i.e., only a section of the wire takes part in the transition. This is an important difference with respect to our calculations where the transition takes place throughout the system in a quite homogeneous way. In our case the fluctuations of the particles around the Wigner peaks are a combined effect of the broken translational symmetry induced by the external confining potential and the strong correlations which causes the particles to repel each other. A nonhomogeneous behavior is found at the edge of the wire where the confining potential in Eq. (14) turns upward. As one can see in Fig. 11, the density variations are larger near the edge, which can be understood in terms of a local mean-field description. At the edge of the wire the effective chemical potential $\mu_0-V(x)$ is smaller, corresponding locally to a fluid at much lower density.

Apart from these features, we did not find any evidence for a Wigner correlated patch embedded in a liquidlike system, although these seem to be found in the experiments. Therefore it may be essential to take into account other factors that can affect the experimental results. For instance, one of the top metallic gates used to tune the upper wire density could induce a plateau in the external potential, nucleating a Wigner region as suggested in Refs. 30 and 53. Notice however that the densities of our homogeneous system should be compared with the densities at the plateau, which are experimentally determined.[12] On the other hand, the role of disorder is not clear. Although in the liquid phase the system is in a ballistic regime, when the conductance is quantized the disorder could take over in the localized phase and affect the charge distribution in the wire. AlAs wires, where the disorder is stronger, revealed conductance resonances explained in terms of Coulomb blockade (CB) physics.[54] CB behavior has also been found in the localized phase of GaAs wires.[12]

Even if there are features that still need explanation, our calculations show that the electronic correlation plays a very important role at the experimental conditions, as the $2k_F$-to-$4k_F$ correlations transition takes place exactly in the proximity of the critical density for localization found in the experiment. In addition to this result, which is the main outcome of the paper, we also determined the charge and spin velocities by means of the QMC method explained in Sec. II and the effective J coupling via the WKB approach. We computed those quantities close to the transition for the homogeneous wire with $r_s=1.25$ (40 μm^{-1}). The charge velocity turns out to be $v_\rho=2.33v_F$. The corresponding LL param-

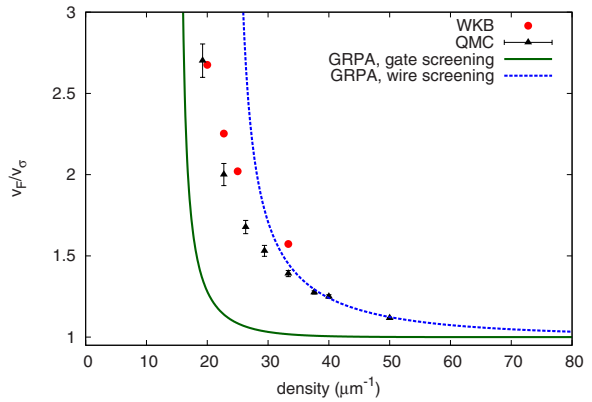

FIG. 12. (Color online) Inverse spin velocity of the infinite wire. The red circles indicate estimates from the WKB approximation, whereas the black triangles are determined using the QMC method described in Sec. II. The two lines are estimates due to the perturbative generalized random-phase approximation (Ref. 55) $v_F/v_\sigma^{\mathrm{GRPA}}=1/\sqrt{1-V(2k_F)/(\pi v_F)}$. The green line for the gated wire (with $R=50$) uses the potential described by Auslaender *et al.* (Ref. 10) whereas the dotted blue line uses the potential [Eq. (12)] screened by the lower wire.

eter $g=v_F/v_\rho=0.43$ is in agreement with previous estimates[31] and comparable to the experimental $g\approx 0.5$, measured at the density of 40 μm^{-1}.[10] At the same density the experimental value for v_F/v_σ is in the range of 1.1–1.6, while we found $v_F/v_\sigma=1.24$ at 40 μm^{-1}.

In Fig. 12 we plot the full dependence of the spin velocities on the density computed with the perturbative generalized RPA (GRPA),[55] WKB, and the exact QMC methods. Although the GRPA is poor near the localization transition, it agrees with the QMC at high density. As noted above the experimentally measured spin velocities are also in rough agreement with the QMC estimate in a range of densities around $n=40$ μm^{-1}. To show the importance of the microscopic details of the interaction in reproducing the measured values we also display in Fig. 12 the GRPA prediction based on a different model potential which assumes a screening due to a metallic gate at $R=50$.[10] This latter model gives virtually unrenormalized spin velocities ($v_\sigma\approx v_F$) up to $n=40$ μm^{-1} in contrast with the strong suppression of the values found in the experiment. For the microscopic details which determine the spin velocities the thickness also plays a very important role, as it sets the short-range behavior of the interaction, and thus the value of J for the effective spin model.

Last but not least, our WKB estimate of J turns out to be of the order of the experimental temperature ($T=0.25$ K) around $n=10$ μm^{-1}. This means that at least the first few Coulomb blockade peaks in the experiment should be in a spin incoherent regime, where the LL description by Fiete *et al.* applies, although in the vicinity of the transition the spin degrees of freedom are not dominated by thermal broadening.

V. CONCLUSIONS

We have presented extensive quantum Monte Carlo calculations to study the properties of electrons constrained to one dimension with a harmonic confinement and interacting via several different potentials.

For unscreened interactions with a long-range $1/x$ tail there are three different regimes. At high density the electrons behave as a correlated liquid, transitioning to a quasi-Wigner crystal as the density decreases, where strong $4k_F$ correlations follow the LL predictions.[23] We accurately determined the crossover density for various thicknesses and found that the crossover is pushed to higher densities for thinner wires. Finally at very low densities the charge degrees of freedom are described by spinless fermions and the spins decouple with exponentially small exchange interactions. We approached this limit by using the WKB approximation.

When screening is introduced, the interactions are not long range and the quasi-Wigner crystal order is destroyed. However, $4k_F$ correlations are still present even in the case of screened interactions. The spinless fermion regime acquires a new behavior when the wire is very thin and the screening makes the potential short range. In this case the particles act as though they were noninteracting and spinless in analogy to physics previously studied for bosons with an infinite contact repulsion.[26]

We applied our numerical approach to analyze a model chosen to realistically describe the double wire system studied in the experiments of Steinberg *et al.*,[12] where a localization transition is observed. Our model assumes screening due to a second wire described within linear-response theory and includes the finite length of the wire via the external potential derived in Ref. 8. We show that a crossover from a liquid to a state with $4k_F$ correlations occurs around the localization density found in the experiment. Additionally, our exact Monte Carlo calculations yield charge and spin velocities for this model in agreement with those observed in the experiment close to the transition. We stress that the observables such as the transition density and the spin velocity are particularly sensitive to the microscopic details of the model interaction. To reproduce all features of the experiment it may be necessary to include further refinements such as a more accurate modulation of the external potential due to the gates, the effects of higher subbands in the transverse direction, and the full treatment of interwire electronic correlation by explicitly including the electrons in the other wire. However, the simple model considered here shows that the exact treatment of electronic correlation is essential to quantitatively describe the localization transition seen in experiments.

ACKNOWLEDGMENTS

We thank D. M. Ceperley, S. Vishveshwara, O. Auslaender, M. Grayson, and M. Polini for useful discussions. L.S., M.C., and R.M.M. acknowledge support in the form of the NSF under Grant No. DMR-0404853.

[1] J. M. Luttinger, J. Math. Phys. **4**, 1154 (1963).
[2] S. Tomonaga, Prog. Theor. Phys. **5**, 554 (1963).
[3] J. Voit, Rep. Prog. Phys. **58**, 977 (1995).
[4] A. M. Chang, Rev. Mod. Phys. **75**, 1449 (2003).
[5] T. Giamarchi, *Quantum Physics in One Dimension* (Clarendon, Oxford, 2004).
[6] O. M. Auslaender, A. Yacoby, R. de Picciotto, K. W. Baldwin, L. N. Pfeiffer, and K. W. West, Science **295**, 825 (2002).
[7] Y. Tserkovnyak, B. I. Halperin, O. M. Auslaender, and A. Yacoby, Phys. Rev. Lett. **89**, 136805 (2002).
[8] Y. Tserkovnyak, B. I. Halperin, O. M. Auslaender, and A. Yacoby, Phys. Rev. B **68**, 125312 (2003).
[9] O. M. Auslaender, H. Steinberg, A. Yacoby, Y. Tserkovnyak, B. I. Halperin, R. de Picciotto, K. W. Baldwin, L. N. Pfeiffer, and K. W. West, Solid State Commun. **131**, 657 (2004).
[10] O. M. Auslaender, H. Steinberg, A. Yacoby, Y. Tserkovnyak, B. I. Halperin, K. W. Baldwin, L. N. Pfeiffer, and K. W. West, Science **308**, 88 (2005).
[11] A. Yacoby, O. M. Auslaender, H. Steinberg, Y. Tserkovnyak, B. I. Halperin, K. W. Baldwin, L. N. Pfeiffer, and K. W. West, Phys. Status Solidi B **243**, 3593 (2006).
[12] H. Steinberg, O. M. Auslaender, A. Yacoby, J. Qian, G. A. Fiete, Y. Tserkovnyak, B. I. Halperin, K. W. Baldwin, L. N. Pfeiffer, and K. W. West, Phys. Rev. B **73**, 113307 (2006).
[13] W. M. C. Foulkes, L. Mitas, R. J. Needs, and G. Rajagopal, Rev. Mod. Phys. **73**, 33 (2001).
[14] P. J. Reynolds, D. M. Ceperley, B. J. Alder, and W. A. Lester, J. Chem. Phys. **77**, 5593 (1982).
[15] C. J. Umrigar, M. P. Nightingale, and K. J. Runge, J. Chem. Phys. **99**, 2865 (1993).
[16] M. Casula, C. Filippi, and S. Sorella, Phys. Rev. Lett. **95**, 100201 (2005).
[17] W. Häusler, L. Kecke, and A. H. MacDonald, Phys. Rev. B **65**, 085104 (2002).
[18] M. Casula, S. Sorella, and G. Senatore, Phys. Rev. B **74**, 245427 (2006).
[19] E. P. Wigner, Phys. Rev. **46**, 1002 (1934).
[20] P. Nozières and D. Pines, *The Theory of Quantum Liquids*, 3rd ed. (Perseus, Cambridge, MA, 1999).
[21] D. M. Ceperley and B. J. Alder, Phys. Rev. Lett. **45**, 566 (1980).
[22] B. Bernu, L. Candido, and D. M. Ceperley, Phys. Rev. Lett. **86**, 870 (2001).
[23] H. J. Schulz, Phys. Rev. Lett. **71**, 1864 (1993).
[24] M. Fogler, Phys. Rev. Lett. **94**, 056405 (2005).
[25] M. M. Fogler, Phys. Rev. B **71**, 161304(R) (2005).
[26] M. Girardeau, J. Math. Phys. **1**, 516 (1960).
[27] W. Häusler and B. Kramer, Phys. Rev. B **47**, 16353 (1993).
[28] K. Jauregui, W. Hauseler, and B. Kramer, Europhys. Lett. **24**, 581 (1993).
[29] K. Jauregui, W. Häusler, D. Weinmann, and B. Kramer, Phys. Rev. B **53**, R1713 (1996).
[30] E. J. Mueller, Phys. Rev. B **72**, 075322 (2005).
[31] G. A. Fiete, J. Qian, Y. Tserkovnyak, and B. I. Halperin, Phys. Rev. B **72**, 045315 (2005).
[32] A. Javey, H. Kim, M. Brink, Q. Wang, A. Ural, J. Gu, P. McIntyre, P. McEuen, M. Lundstrom, and H. Dai, Nature Mater. **1**, 241 (2002).
[33] B. M. Kim, T. Brintlinger, E. Cobas, M. S. Fuhrer, H. Zheng, Z. Yu, R. Droopad, J. Ramdani, and K. Eisenbeiser, Appl. Phys. Lett. **84**, 1946 (2004).
[34] K. X. Liu, M. H. Kalos, and G. V. Chester, Phys. Rev. A **10**, 303 (1974).
[35] M. Calandra Buonaura and S. Sorella, Phys. Rev. B **57**, 11446 (1998).
[36] T. Gaskell, Proc. Phys. Soc. London **77**, 1182 (1961).
[37] A. Gold and L. Calmels, Solid State Commun. **96**, 101 (1995).
[38] M. Casula and G. Senatore, ChemPhysChem **6**, 1902 (2005).
[39] T. Giamarchi and H. J. Schulz, Phys. Rev. B **39**, 4620 (1989).
[40] L. Shulenburger, M. Casula, G. Senatore, and R. M. Martin (unpublished).
[41] A. Gold and L. Calmels, Phys. Rev. B **58**, 3497 (1998).
[42] D. M. Ceperley and B. Bernu, J. Chem. Phys. **89**, 6316 (1988).
[43] R. P. Feynman and M. Cohen, Phys. Rev. **102**, 1189 (1956).
[44] K. A. Matveev, Phys. Rev. B **70**, 245319 (2004).
[45] J. des Cloizeaux and J. J. Pearson, Phys. Rev. **128**, 2131 (1962).
[46] L. D. Faddeev and L. A. Takhtajan, Phys. Lett. **85A**, 375 (1981).
[47] A. D. Klironomos, R. R. Ramazashvili, and K. A. Matveev, Phys. Rev. B **72**, 195343 (2005).
[48] M. M. Fogler and E. Pivovarov, Phys. Rev. B **72**, 195344 (2005).
[49] M. Fogler and E. Pivovarov, J. Phys.: Condens. Matter **18**, L7 (2006).
[50] S. Sorella, Phys. Rev. B **64**, 024512 (2001).
[51] Michele Casula, Claudio Attaccalite, and Sandro Sorella, J. Chem. Phys. **121**, 7110 (2004).
[52] W. Häusler and B. Kramer, Phys. Rev. B **47**, 16353 (1993).
[53] J. Qian and B. I. Halperin, Phys. Rev. B **77**, 085314 (2008).
[54] J. Moser, S. Roddaro, D. Schuh, M. Bichler, V. Pellegrini, and M. Grayson, Phys. Rev. B **74**, 193307 (2006).
[55] C. E. Creffield, W. Häusler, and A. H. MacDonald, Europhys. Lett. **53**, 221 (2001).